Atmos. Chem. Phys., 23, 9439–9453, 2023
https://doi.org/10.5194/acp-23-9439-2023

Atmospheric Chemistry and Physics
Open Access
EGU

Concurrent photochemical whitening and darkening of ambient brown carbon

Qian Li[1], Dantong Liu[1], Xiaotong Jiang[1], Ping Tian[2], Yangzhou Wu[1], Siyuan Li[1], Kang Hu[1], Quan Liu[3], Mengyu Huang[2], Ruijie Li[2], Kai Bi[2], Shaofei Kong[4], Deping Ding[2], and Chenjie Yu[5]

[1]Department of Atmospheric Science, School of Earth Sciences, Zhejiang University, Hangzhou, 310027, China
[2]Beijing Key Laboratory of Cloud, Precipitation and Atmospheric Water Resources, Beijing Meteorological Service, Beijing, 100089, China
[3]State Key Laboratory of Severe Weather & Key Laboratory of Atmospheric Chemistry of CMA, Chinese Academy of Meteorological Sciences, Beijing, 100081, China
[4]Department of Atmospheric Science, School of Environmental Studies, China University of Geosciences, Wuhan, 430074, China
[5]LISA, CNRS, Université de Paris Cité and Université Paris Est Creteil, Paris, France

Correspondence: Dantong Liu (dantongliu@zju.edu.cn)

Received: 6 July 2022 – Discussion started: 18 July 2022
Revised: 29 June 2023 – Accepted: 13 July 2023 – Published: 25 August 2023

Abstract. The light-absorbing organic aerosol (OA), known as brown carbon (BrC), has important radiative impacts; however, its sources and evolution after emission remain to be elucidated. In this study, the light absorption at multiple wavelengths, mass spectra of OA and microphysical properties of black carbon (BC) were characterized at a typical suburban environment in Beijing. The absorption of BC is constrained by its size distribution and mixing state, and the BrC absorption is obtained by subtracting the BC absorption from the total aerosol absorption. Aerosol absorption was further apportioned to BC, primary BrC and secondary BrC by applying the least correlation between secondary BrC and BC. The multilinear regression analysis on the factorized OA mass spectra indicated that the OA from traffic and biomass burning emission contributed to primary BrC. Importantly, the moderately oxygenated OA (O / C = 0.62) was revealed to highly correlate with secondary BrC. These OA had higher nitrogen content, in line with the nitrogen-containing functional groups detected by the Fourier transform infrared spectrometer. The photochemical processes were found to reduce the mass absorption cross section (MAC) of primary OA, reducing its contribution to total absorption by 20 %, at the same time increasing MAC for secondary OA, which showed a 30 % enhancement in contribution to total absorbance, implying the concurrent whitening and darkening of BrC. This provides field evidence that the photochemically produced secondary nitrogen-containing OA can considerably compensate for some bleaching effect on the primary BrC, hereby causing radiative impacts.

1 Introduction

Atmospheric absorbing organic aerosol (OA), known as brown carbon (BrC), is an important contributor to anthropogenic absorption besides black carbon (BC) (Laskin et al., 2015; Liu et al., 2020), particularly at shorter visible wavelengths (Bahadur et al., 2012). Due to complex compositions of OA, the primary sources and subsequent evolution of BrC in the atmosphere remains to be explicitly understood and causes uncertainties in evaluating the radiative impacts of BrC (Liu et al., 2020).

The chromophores of BrC are mainly aromatic compounds associated with certain functional groups (P. F. Liu et al., 2015). Particularly, compounds containing nitro, nitrated or other forms of nitrogen-containing functional groups are

more absorbing (Nakayama et al., 2013; Jacobson, 1999). It is well established that primary OA, especially from biomass burning, contains a large fraction of BrC (Andreae and Crutzen, 1997; Rizzo et al., 2013; Bond, 2001). These primary BrC have a range of absorptivity, which was found to be controlled by burning phases. OA co-emitting with BC (the flaming phase) exhibited a higher absorptivity than an OA-dominated smoldering phase (Liu et al., 2021). BrC can experience reactions with atmospheric oxidants after emission. Previous studies (Satish et al., 2017; Satish and Rastogi, 2019; Dasari et al., 2019) found nitrogenous compounds from biomass burning were responsible for BrC over South Asia, and the chromophores were photobleached in the afternoon. Numerous field and laboratory studies found the decrease of BrC absorptivity due to photobleaching of chromophores, with the lifetime ranging from a few hours (Zhao et al., 2015; Liu et al., 2021) to a few days (Forrister et al., 2015), which may depend on the concentration of ambient hydroxyl radical (Wang et al., 2014), also influenced by relative humidity and particle volatility (Schnitzler et al., 2020). The absorptivity of BrC could also be enhanced due to the addition of functional groups by forming a conjugated structure with aromatics. This was supported by a number of laboratory studies that BrC absorptivity could be enhanced when forming nitrogen-containing organic compounds, such as the formation of nitro-aromatics when aromatics reacted with NO_x (Nakayama et al., 2013) or produced organic amine after reacting with ammonia (Updyke et al., 2012). The enhancement of BrC absorptivity could occur either through the nitration of existing chromophores or the formation of new secondary organic aerosol (SOA) chromophores through gas-phase oxidation.

The above findings mean the enhancement or bleaching of BrC absorptivity via photochemical processes will coexist. The timescale between both competing processes will ultimately determine the lifetime of BrC in the atmosphere. However, both processes have rarely been investigated in the field to explicitly determine the BrC components which principally determine the respective enhancement or decrease of its absorptivity, particularly in regions influenced by combined anthropogenic sources.

In this study, by measurements using multiple-wavelength absorption and microphysical properties of BC in a suburban region, the absorption of BC, primary BrC and secondary BrC was discriminated. In conjunction with source attribution via OA mass spectra, we are able to link the segregated absorption with certain sources and investigate their primary information and subsequent evolution. The competition between photobleaching and secondary formation of BrC was investigated in the real world.

2 Experimental and instrumentation

2.1 Site description and meteorology

The experiment was conducted during springtime at the Beijing Cloud Laboratory and Observational Utilities Deployment Base (117.12° E, 40.14° N), which is located in the northeast suburban area in Beijing (Fig. S1a in the Supplement). The site is surrounded by the northwest mountain ridge, without significant local primary anthropogenic emissions (Hu et al., 2021). The 72 h backward trajectories with every 3 h initializing from the site are analyzed by the HYSPLIT model (Draxier and Hess, 1998) using the 3-hourly $1° \times 1°$ meteorological field from the Global Data Assimilation System (GDAS) reanalysis product. The obtained backward trajectories were further clustered to group the similar transport pathways (Makra et al., 2011). The meteorological parameters, including the temperature (T), ambient relative humidity (RH), wind speed (WS) and wind direction (WD), were measured by a monitoring station on the site.

2.2 Measurements of BC microphysics and absorption coefficient

In this study, the ambient aerosols were sampled by a large-flow ($1.05\,m^3\,min^{-1}$) air particle sampler (Th-1000C II) with a $PM_{2.5}$ impactor (BGI SCC 1.829) and dried by a silica drier before measurement. The single particle soot photometer (SP2, DMT., USA) used a continuous laser at $\lambda = 1064$ nm to incandesce light-absorbing aerosols (such as BC) for irradiating detectable visible light. The incandescence signal was used to measure the refractory black carbon (rBC) mass. The SP2 incandescence signal was calibrated using the Aquadag standard (Acheson Inc., USA), and a factor of 0.75 was applied to correct for ambient BC (Laborde et al., 2012). The scattering signal was calibrated by monodispersed polystyrene latex spheres (PSLs). The BC core diameter (D_c) was calculated from the measured BC mass by assuming a BC density of $1.8\,g\,cm^{-3}$ (Bond and Bergstrom, 2006). The leading edge only (LEO) method was applied to reconstruct the scattering signal of BC, which was used to determine the coated particle diameter (D_p) by a Mie lookup table with the inputs of scattering and the incandescence signal of each BC particle (Liu et al., 2014; Taylor et al., 2015). The mass median diameter (MMD) is derived from the D_c distribution, which is determined as below, and above the MMD the rBC mass concentration is equal (Liu et al., 2019). The bulk coating thickness (D_p/D_c) is calculated as the cubic root of ratio of the total coated BC volume divided by the total volume of rBC.

The mass absorption cross section (MAC) (in $m^2\,g^{-1}$) of each BC particle can be calculated using the measured coated and uncoated BC sizes by applying the Mie core–shell calculation. The absorption coefficient of BC at certain wavelength, $\sigma_{abs,BC}$ (λ), is determined by multiplying the calcu-

lated MAC and rBC mass concentration at each size:

$$\sigma_{\mathrm{abs,BC}}(\lambda) = \sum_i \mathrm{MAC}\left(\lambda, D_{\mathrm{p},i}\, D_{\mathrm{c},i}\right) m\left(\log D_{\mathrm{c},i}\right) \Delta \log D_{\mathrm{c},i}, \quad (1)$$

where $m(\log D_{\mathrm{c},i})$ denotes the BC mass concentration at each logarithmic bin of D_{c}. The SP2 measurement at $\lambda = 1064$ nm longer than the mostly populated BC size means the derived coatings and subsequent calculation of MAC is relatively independent of particle shape within an uncertainty of 21 % (Liu et al., 2014; Hu et al., 2021).

The absorption coefficients at wavelengths $\lambda = 375$, 470, 528, 635 and 880 nm were measured by a microaethalometer (microAeth, MA200, AethLabs, San Francisco, CA, USA). Aerosol particles were collected on filter tapes, on which the light attenuation was measured continuously with a time resolution of 30 s. The loading effect of filters was automatically corrected by measuring attenuation at two different sampling flow rates on two spots in parallel (Drinovec et al., 2015). Moreover, a multi-scattering correction factor (C value) of 3.5, 3.2 and 2.4 at the wavelengths 370, 528 and 880 nm, respectively, were utilized to correct attenuation for the multiple light scattering effect. It was obtained by comparing the absorption coefficient with a photoacoustic soot spectrometer (PASS-3, DMT) (Hu et al., 2021).

2.3 Attribution of primary and secondary BrC absorption coefficient

The absorption coefficient of BC at different λ is calculated using the measured uncoated core and coated size as mentioned above. The absorption coefficient of total BrC is obtained by subtracting the BC absorption coefficient from the total absorption at certain wavelength, expressed as

$$\sigma_{\mathrm{abs,BrC}}(\lambda) = \sigma_{\mathrm{abs,total}}(\lambda) - \sigma_{\mathrm{abs,BC}}(\lambda), \quad (2)$$

where the absorption coefficient of BC ($\sigma_{\mathrm{abs,BC}}$) is obtained from the SP2 measurement, and $\sigma_{\mathrm{abs,total}}$ (λ) is the total light absorption of aerosols measured by the MA200. The absorption coefficient of secondary BrC, the absorption not contributed by primary sources, is obtained by subtracting the absorption of all primary sources from the total absorption (Crilley et al., 2015), expressed as

$$\sigma_{\mathrm{abs,secBrC}}(\lambda) = \sigma_{\mathrm{abs,total}}(\lambda) - \sigma_{\mathrm{abs,pri}}(\lambda), \quad (3)$$

where $\sigma_{\mathrm{abs,pri}}$ (λ) is the light absorption from primary sources. Here an assumption is made that light absorption from primary aerosols is all from combustion sources, and these sources necessarily contain BC (Q. Wang et al., 2018). Therefore, the total absorption from primary sources can be obtained by scaling a factor from the mass concentration of BC, expressed as

$$\sigma_{\mathrm{abs,pri}}(\lambda) = \left(\frac{\sigma_{\mathrm{abs,total}}}{[\mathrm{rBC}]}\right)_{\mathrm{pri}} \cdot [\mathrm{rBC}], \quad (4)$$

where [rBC] is the mass concentration of rBC measured by the SP2, and $\left(\frac{\sigma_{\mathrm{abs,total}}}{[\mathrm{rBC}]}\right)_{\mathrm{pri}}$ is the scaling factor to derive the absorption of primary combustion sources from [rBC]. This factor is obtained using the minimum R-squared (MRS) approach (Wu and Yu, 2016) by adjusting the factor until a minimum correlation between $\sigma_{\mathrm{abs,secBrC}}$ and [rBC] is reached because the absorption from secondary sources are least likely to covary with that from primary sources (Q. Wang et al., 2019a). This method has been used in urban and suburban environments to obtain the primary BrC associated with combustion sources. Being different from previous studies, an auxiliary characterization of rBC mass measured by the SP2 is used here to avoid the possible interference from absorption measured by the same instrument. There may be a different $\left(\frac{\sigma_{\mathrm{abs,total}}}{[\mathrm{rBC}]}\right)_{\mathrm{pri}}$ ratio between traffic and biomass burning sources, and this may lead to bias in deriving the subsequent results. We have more carefully investigated the diurnal pattern of hydrocarbon-like OA (HOA) and biomass burning OA (BBOA) and found only a slight morning rush hour peak for HOA (though bearing considerable variation). A further investigation on the HOA/BBOA ratio found no apparent diurnal pattern (bearing large variation), shown in Fig. S8. The source difference is therefore not considered to have significantly influenced the diurnal pattern of derived parameters. In addition, this method is only valid with sufficient data points; thus, we may only obtain a single mean value for the entire experiment, which represents the mean $\left(\frac{\sigma_{\mathrm{abs,total}}}{[\mathrm{rBC}]}\right)_{\mathrm{pri}}$ in this environment during the experimental period. Previous studies using this method also derived the mean value of $\left(\frac{\sigma_{\mathrm{abs,total}}}{[\mathrm{rBC}]}\right)_{\mathrm{pri}}$ for the urban environment influenced by multiple sources including traffic, coal combustion and biomass burning (Q. Wang et al., 2019b, 2020; Gao et al., 2022). The $\left(\frac{\sigma_{\mathrm{abs,total}}}{[\mathrm{rBC}]}\right)_{\mathrm{pri}}$ ratio at $\lambda = 375$, 470, 528, 635 and 880 nm is calculated to be 20.7, 17.0, 14.4, 11.7 and 5, respectively (Fig. S2), which falls within the reported values from previous studies 11–50 (Zhang et al., 2020; Q. Wang et al., 2019a). This scenario assumes a relatively consistent absorption relative to BC mass concentration from sources during the experiment. This however may not include some sporadic events when sources with distinct OA or BC mass fractions may be introduced and alter the single $\left(\frac{\sigma_{\mathrm{abs,total}}}{[\mathrm{rBC}]}\right)_{\mathrm{pri}}$ ratio. The $\sigma_{\mathrm{abs,secBrC}}$ therefore represents the overall mean value during the experimental period, but this ratio will vary with seasons and locations. The σ_{abs} of primary BrC can then be calculated as

$$\sigma_{\mathrm{abs,priBrC}}(\lambda) = \sigma_{\mathrm{abs,BrC}}(\lambda) - \sigma_{\mathrm{abs,secBrC}}(\lambda), \quad (5)$$

where $\sigma_{\mathrm{abs,BrC}}$ and $\sigma_{\mathrm{abs,secBrC}}$ is calculated from Eqs. (2) and (3), respectively.

2.4 Composition measurement

The mass concentration and chemical composition of non-refractory submicron PM (NR-PM_1) including organic aerosols (OAs), nitrate (NO_3^-), sulfate (SO_4^{2-}), chloride (Cl^-) and ammonium (NH_4^+) were determined with a High-Resolution Time-of-Flight Aerosol Mass Spectrometer (HR-ToF-AMS, Aerodyne Research Inc., USA). The setup, operation and calibration procedures of the AMS have been described elsewhere (Canagaratna et al., 2007). During this field observation, the AMS was operated in V-mode for the quantification of mass concentrations. The composition-dependent collection efficiencies were applied (Middlebrook et al., 2012), and the ionization efficiency was calibrated using 300 nm of pure ammonium nitrate (Jayne et al., 2000). Elemental ratios of OA including oxygen-to-carbon (O / C), hydrogen-to-carbon (H / C) and nitrogen-to-carbon (N / C) were determined to the improved-ambient method (Canagaratna et al., 2015).

Positive matrix factorization (PMF) (Paatero and Tapper, 1994) was performed on the inorganic and organic high-resolution mass spectra to distinguish OA components from different sources (Zhang et al., 2011; Ulbrich et al., 2009; Decarlo et al., 2010). The mass spectra of the combined matrix for $m/z < 120$ were excluded in PMF analysis. Five OA factors were identified. The diagnostics of PMF are summarized in Text S1 and Fig. S6.

2.5 Offline Fourier transform infrared spectrometer (FTIR) analysis

Particulate matter (PM) samples were collected once a day onto prebaked (600 °C, 4 h) quartz fiber filters (Whatman, QM-A, USA) using a large-flow (1.05 $m^3\,min^{-1}$) air particle sampler (Th-1000C II). The collected filter samples were stored in the refrigerator at −20 °C before analysis. The infrared spectra of collected samples were measured by a Fourier transform infrared spectrometer (FTIR, Thermo Fisher Scientific, USA) equipped with an iD5 attenuated total reflectance accessory (diamond crystal) to quantify the chemical functional groups over the wavenumber range of 550–4000 cm^{-1} with a resolution of 0.5 cm^{-1}. The NO and NO_2 symmetric stretch in the FTIR spectra can characterize the functional groups associated with nitrogen-containing organics (Coury and Dillner, 2008). Figure S3 shows typical examples of FTIR spectra and the assigned functional groups for the three pollution levels during experiment. The peak at 1110 cm^{-1} corresponds to the background of the quartz fiber filter overlapped with some X–H bending vibrations, which are subtracted for the following analysis. The characteristic organic nitrate spectra appear at wavenumbers 860 cm^{-1} (NO symmetric stretch), 1280 cm^{-1} (NO_2 symmetric stretch) and 1630–1640 cm^{-1} (NO_2 asymmetric stretch) (Bruns et al., 2010). After baseline calibration, the FTIR peaks of 1630 and 860 cm^{-1} are integrated into the absorption areas above the baseline. The summed integrated areas of -NO and -NO_2 are hereby used to indicate the nitrogen-containing organics. There was no discernable peak of a carbonyl group for our infrared spectrum, and the peak of OH at 2500–3400 cm^{-1} for the carboxylic acid is not discernable either; thus, the influence of ketone and carboxylic acid may be of less importance for our dataset.

3 Results and discussion

3.1 Source-attributed OA

The overview results are shown in Fig. S1. The organics dominated the aerosol compositions for the most time, but occasionally nitrate was the most abundant component (Fig. S1g). Note that the nitrate here may also include components containing organics besides ammonium nitrate. Backward trajectories (Fig. S1a–d) showed that the most abundant PM_1 concentration was associated with air masses transported in shorter distances from southern regions (C1), but the longer and faster northerly transported air mass from cleaner north (C2) could dilute the concentrations.

The resolved OA factors by the PMF analysis are shown in Fig. 1, including the mass spectra, time series and diurnal profiles of each PMF factor with corresponded external and internal tracers. Three primary OA (POA) were identified as HOA, cooking-related OA (COA) and BBOA, with O / C of 0.31, 0.18 and 0.39, respectively. These POA had considerable fraction of hydrocarbon fragments (C_xH_y), indicating their less aged status. The HOA profile was characterized by higher contributions of aliphatic hydrocarbons and has dominated ion tracers such as m/z 41 ($C_3H_5^+$), 43 ($C_3H_7^+$), 55 ($C_4H_7^+$) and 57 ($C_4H_9^+$). The HOA concentration correlated with BC ($r = 0.62$), which emits from traffic emissions. The diurnal variation exhibited strong morning and afternoon rush hour peaks of mass concentration. This factor was consistent with the mass spectra of previously measured HOA from on-road vehicle emissions in urban cities (Zhang et al., 2005; Aiken et al., 2009; Sun et al., 2016; Hu et al., 2017), which have m/z peaks characteristic of hydrocarbon fragments in series of $C_nH_{2n+1}^+$ and $C_nH_{2n-1}^+$. The mass spectrum of HOA shows an overall similarity to those of primary OA emitted from gasoline and diesel combustion sources ($r = 0.68$) (Elser et al., 2016).

The OA from cooking sources (COA) is also characterized by prominent hydrocarbon ion series, however, with higher signal at $C_nH_{2n-1}^+$ than $C_nH_{2n+1}^+$. COA had apparent fragments of both $C_4H_9^+$ and $C_3H_3O^+$ and has a higher ratio of $C_3H_3O^+$ / $C_3H_5O^+$ (3.1) and $C_4H_7^+$ / $C_4H_9^+$ (2.2) than HOA (0.9–1.1), with cooking-related fragments of $C_5H_8O^+$ (m/z 84), $C_6H_{10}O^+$ (m/z 98) and $C_7H_{12}O^+$ (m/z 112) (Sun et al., 2011b; Mohr et al., 2012). The COA shows an overall similar spectral pattern to the reference spectra of COA ($r = 0.92$) (Elser et al., 2016). Its minor peak at noon and larger peak in the evening (Fig. 1l) also corresponded with

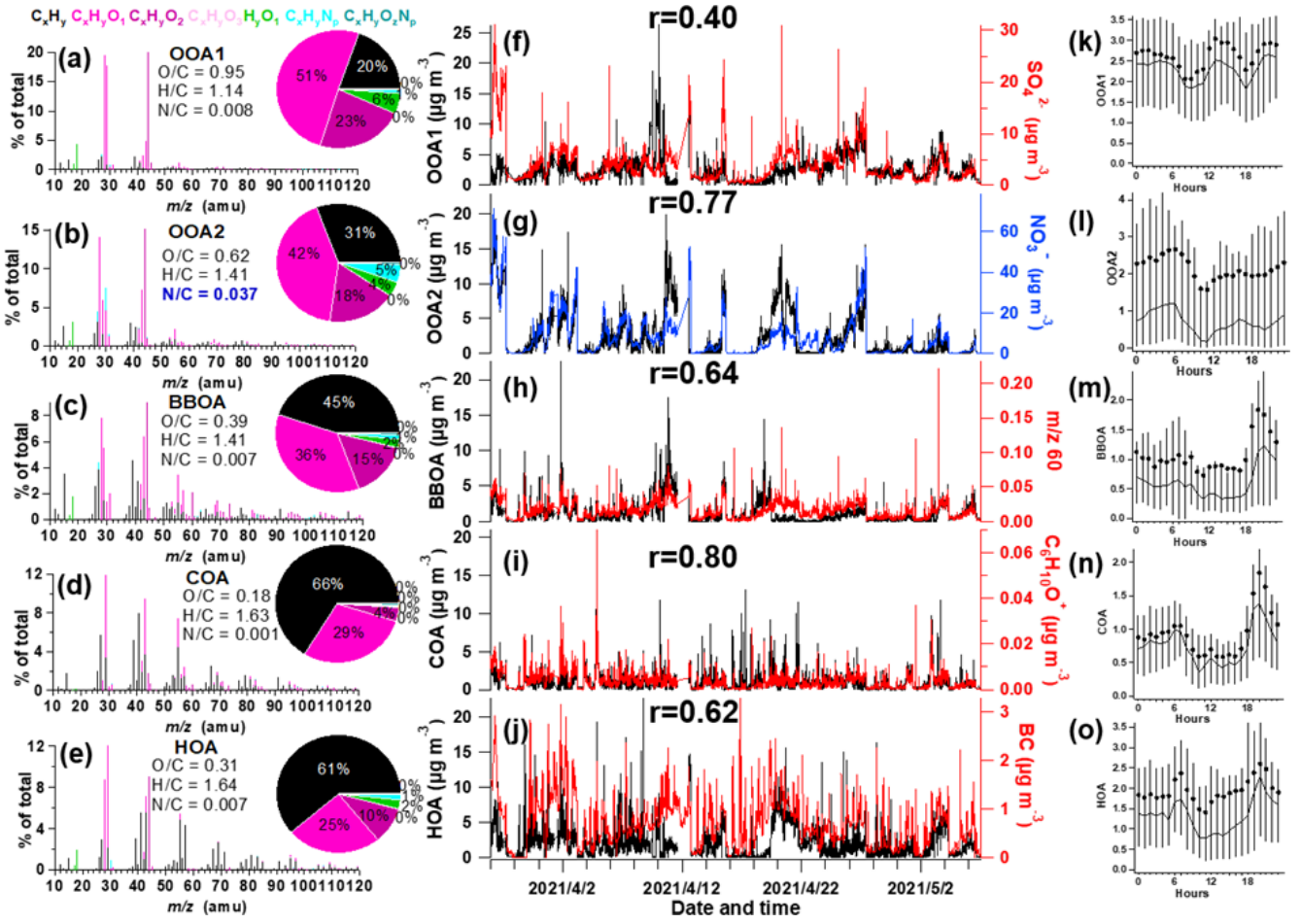

Figure 1. Information of source-apportioned organic aerosols by the PMF analysis. Mass spectra of **(a)** oxygenated OA1 (OOA1), **(b)** oxygenated OA2 (OOA2), **(c)** biomass burning OA (BBOA), **(d)** cooking-related OA (COA), **(e)** hydrocarbon-like OA (HOA), and **(f–j)** temporal variations of each PMF factor and the corresponding marker species. **(k–o)** Diurnal profiles of each factor. The lines, dots and whiskers denote the median, mean and 25th/75th percentiles at each hour, respectively.

the lunch and dinner time, respectively. There was only a minor peak at noon for COA, which may be due to the suburban nature of the site where the major aerosols from cooking sources may have been processed and lost the signature near the source. The feature of this factor was also observed in the suburban environment (Huang et al., 2021).

The BBOA factor was identified based on the prominent signals of m/z 60 ($C_2H_4O_2^+$) and 73 ($C_3H_5O_2^+$), which are known fragments of levoglucosan (Cubison et al., 2011). And BBOA also correlated with potassium (K^+, $r = 0.80$), which is an indicator of biomass burning (Pachon et al., 2013; Brown et al., 2016). The m/z 60 and 73 together with a unique diurnal variation have been shown to be a robust marker for the presence of aerosols from biomass burning emissions in many urban locations (Sun et al., 2016). The BBOA shows very similar mass spectral patterns to previously reported reference spectra of biomass burning ($r = 0.94$) (Elser et al., 2016). The BBOA factor that was identified in spring accounted for 12.8 % of the total OA in Beijing, similar to previous reports (Hu et al., 2017). Biomass (Cheng et al., 2013) and solid fuel burning emissions (Sun et al., 2014) have been widely observed to contribute importantly to the primary OA in this region. This off-road combustion source was particularly abundant during wintertime for residential heating activities (Shen et al., 2019; Yang et al., 2018; Liu et al., 2016), while a boiler for industry use (mostly using coal as fuel) was in operation throughout the year (F. Liu et al., 2015). During the springtime of the experiment, the residential heating activities dropped due to increased ambient temperature; thus, the BBOA may be mainly contributed to by the industry sector.

Two types of oxygenated organic aerosols (OOAs) were identified, in moderate (OOA2, O / C = 0.62) and high oxidation state (OOA1, O / C = 0.95), respectively, which is very similar to the spectra of OOA factors resolved in other cities (Hayes et al., 2013; Ulbrich et al., 2009). The average mass spectrum of OOA2 in this study is characterized by m/z 29 (mainly CHO^+), 43 (mainly $C_2H_3O^+$) and

m/z 44 (CO_2^+), similar to the semi-volatile OOA spectrum identified in other locations (Sun et al., 2011a; Zhou et al., 2016). On average, OOA2 accounts for 42 % and 18 % of $C_xH_yO^+$ and $C_xH_yO_2^+$ ions, respectively (Fig. 1b). These results clearly indicate that OOA2 was primarily composed of less oxygenated, possibly freshly oxidized organics. Notably, OOA2 had a substantially higher N / C than other factors (N / C = 0.037), and had the highest correlation with nitrate ($r = 0.77$) and with $C_xH_yN_z$ and $C_xH_yN_zO_p$ fragments ($r = 0.83$). This factor therefore tends to largely result from nitrogen-containing OA, and its elevation at night may be also associated with dark oxidation by nitrate radicals.

The mass spectrum of OOA1, which was characterized by a dominant peak at m/z 44 (mainly CO_2^+), has the highest O / C (0.95). On average, OOA1 contributes 51 % of the $C_xH_yO^+$ signal and 23 % of the $C_xH_yO_2^+$ signal (Fig. 1a). OOA1 showed a particularly high correlation with sulfate ($r = 0.40$) because of their similar volatilities (Huffman et al., 2009; Jimenez et al., 2009). The slight enhancement at noon for OOA1 (also for OOA2) soon after morning rush hour indicated the likely rapid formation of SOA through photochemical processes. This significantly higher mean OOA2 than median value in the diurnal pattern indicated that this OA type was largely associated with pollution events. Both OOA1 and OOA2 showed a nighttime peak that may be due to a reduced boundary layer.

3.2 Segregated aerosol absorption

Figure 2 shows the time series of BC properties, including the BC mass concentration, D_p/D_c, D_c, MAC and light absorption coefficient of BC (Sect. 2.2). The MMD of the BC core varied between 93–274 nm, which may correspond to the source-specific information (Liu et al., 2019) or coagulation process during aging. The coating of BC (indicated by D_p/D_c) showed sporadic enhancement which was closely associated with enhanced PM concentration (Fig. 2a). This was consistent with previous studies that high coatings of BC occurred during heavier pollution due to the enhanced secondary formation of condensable materials to particle phase (Ding et al., 2019; Zhang et al., 2018). This clearly indicates the variation of the mixing state of BC, and this will potentially influence its MAC and absorption Ångström exponent (AAE) (D. Liu et al., 2015). It will introduce considerable uncertainties to use constant MAC or AAE to derive the absorption coefficient of BC at multiple wavelengths. The MAC estimated using the measured BC core size and coatings (Fig. 2c) is thus used to derive the $\sigma_{abs,BC}$ (Sect. 2.2, shown in Fig. 2d). The $\sigma_{abs,BC}$ was $9.1 \pm 7.3\ Mm^{-1}$ during the experimental period. The MAC of BC at $\lambda = 375$ nm was shown to be at 8.4–16.6 $m^2\ g^{-1}$ with enhanced absorption when having a high coating, which was consistent with previous studies which reported a MAC_{BC} of 8–10 $m^2\ g^{-1}$ and a higher value of 9.7–17.2 $m^2\ g^{-1}$ under polluted conditions (Ding et al., 2019; Hu et al., 2021). The uncertainty of $\left(\frac{\sigma_{abs,total}}{[rBC]}\right)_{pri}$ is 4 % for the data points over 1.5 according to Q. Wang et al. (2019a). The measurement of rBC mass from the SP2 had an uncertainty of 20 % (Schwarz et al., 2008), with relative coating thickness having an uncertainty of 23 % (Taylor et al., 2015), hereby resulting in a uncertainty of 27 % for calculated MAC_{BC}. The above results in uncertainties of 31 % and 20 % for $\sigma_{abs,BC}$ and $\sigma_{abs,pri}$, respectively. The absorption measurement by MA200 had an uncertainty of 25 % (Drinovec et al., 2015; Düsing et al., 2019). All these uncertainties propagate the uncertainties of $\sigma_{abs,BrC}$, $\sigma_{abs,priBrC}$ and $\sigma_{abs,secBrC}$ as 40 %, 37 % and 32 %, respectively. These are summarized in Table S1.

Using the method above, the total ($\sigma_{abs,total}$) and attributed absorption of BC ($\sigma_{abs,BC}$), primary BrC ($\sigma_{abs,priBrC}$) and secondary BrC ($\sigma_{abs,secBrC}$) at $\lambda = 375$ nm are shown in Fig. 3a–c. In Fig. 3b, the brown and green shades above the adjacent tracer indicate the absorption coefficient of primary and secondary BrC, respectively. Figure 3c shows that the absorption coefficient of primary BrC was higher than secondary BrC for the most time, but for certain periods they were equivalent or secondary BrC occasionally exceeded primary BrC. The mean contribution of the absorption coefficient for BC, primary BrC and secondary BrC is 51 %, 27 % and 22 % in this study. The tracers associated with nitrogen-containing organics, such as OOA2 (with the highest N / C), $C_xH_yN_z$ and $C_xH_yN_zO_p$ fragments, and the FTIR measured -NO + -NO_2 are also shown in Fig. 3d–e.

3.3 Source attribution of BrC absorption

A multiple linear regression (MLR) analysis is performed to apportion the absorption coefficient of BrC with the PMF attributed OA factors, expressed as

$$\sigma_{abs,BrC} = a_0 + a_1 \cdot [OOA1] + a_2 \cdot [OOA2] + a_3 \cdot [BBOA] + a_4 \cdot [COA] + a_5 \cdot [HOA], \quad (6)$$

where a_1 to a_5 represents the regression coefficient for each factor. These coefficients can be associated with the absorptivity of each factor, i.e., a larger coefficient implies a higher MAC for the source associated with that OA factor (Kasthurirachchi et al., 2020; Wang et al., 2021). The BBOA was found to have the highest MAC at 2.59 $m^2\ g^{-1}$, consistent with previous studies which also found a significantly higher absorption for biomass burning sources (Qin et al., 2018; Q. Wang et al., 2019b; Zhang et al., 2022). The other POA factors generally have a higher MAC than SOA (the MAC of HOA and COA is 1.70 and 1.30 $m^2\ g^{-1}$, respectively). Particularly, the OOA2 has a relatively high MAC of 1.22 $m^2\ g^{-1}$, which is likely to result from the production of secondary BrC, as discussed below. The contribution of each source-specific OA factor to $\sigma_{abs,BrC}$ can also be obtained. This analysis is performed for the total BrC, primary BrC and secondary BrC, respectively. The results are shown in Table 1. The MLR on the total BrC shows a relatively higher correc-

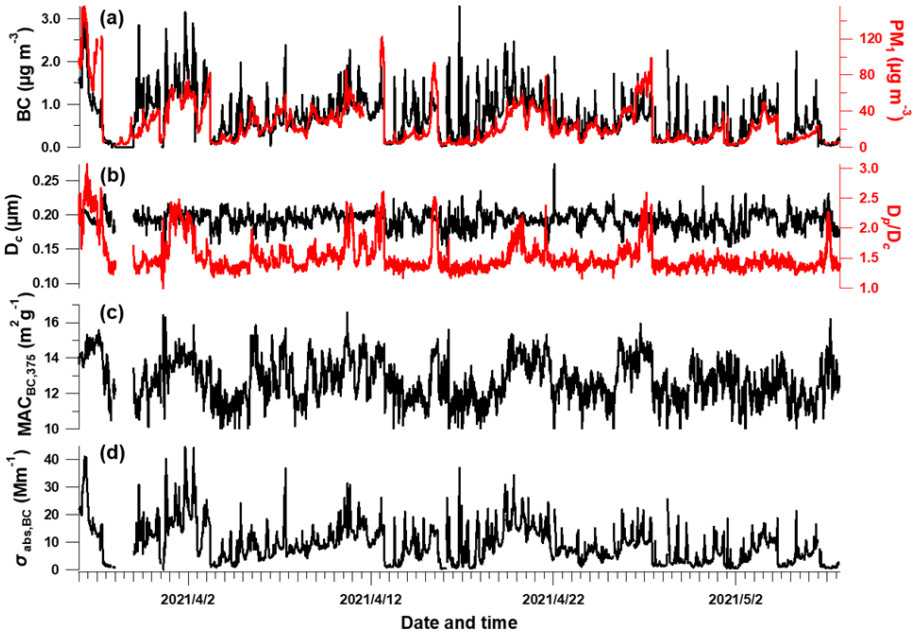

Figure 2. Temporal evolution of BC-related properties. **(a)** rBC and PM_1 mass concentration, **(b)** BC core diameter and bulk coating thickness (D_p/D_c), **(c)** calculated mass absorption cross section (MAC) at $\lambda = 375$ nm and **(d)** absorption coefficient of BC.

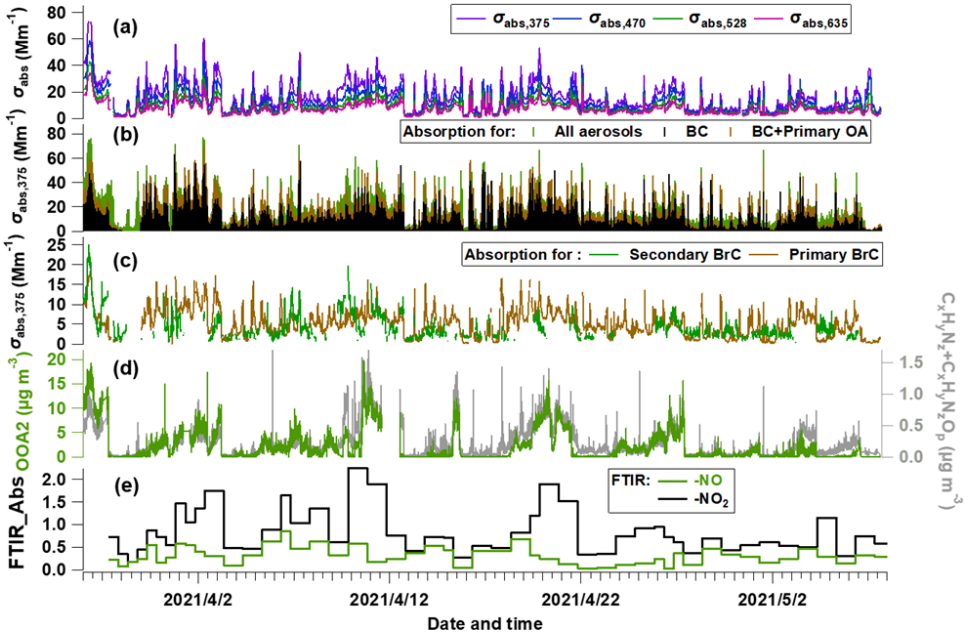

Figure 3. Temporal evolution of segregated absorbing properties. **(a)** Absorbing coefficients (σ_{abs}) at multiple wavelengths measured by the aethalometer; **(b)** σ_{abs} at $\lambda = 375$ nm ($\sigma_{abs,375}$) for all aerosols, primary OA and BC; and **(c)** $\sigma_{abs,375}$ for primary BrC and secondary BrC. **(d)** Mass concentration of OOA2 and the $C_xH_yN_z$ and $C_xH_yN_zO_p$ fragments measured by the AMS. **(e)** FTIR-measured absorption of -NO and -NO_2 bonds.

tion ($r > 0.4$) with the factors of HOA, BBOA and OOA2, suggesting the potential importance of the primary biomass burning and traffic source along with OOA2 in governing the absorption of BrC. MLR analysis on the primary BrC distinguishes its substantial correlation with BBOA ($r = 0.40$) and HOA ($r = 0.46$), while MLR on the secondary BrC has a high correlation with OOA2 only ($r = 0.44$). The MLR analysis links the apportioned absorption of physical properties with source-attributed chemical compositions, therefore val-

idating and identifying the sources of primary and secondary BrC.

Importantly, an oxygenated secondary OA factor (OOA2) is identified as significantly contributing to the secondary BrC. This OOA has a moderate O / C (0.62) and the highest N / C of 0.037 among all factors. The high N / C means this factor contains the most abundant nitrogen-containing fragments, implied by its high correlation with the $C_xH_yN_z$ and $C_xH_yN_zO_p$ fragments ($r = 0.83$, Fig. 3d) and with the FTIR absorption for -NO_2 and -NO bonds ($r = 0.69$, Fig. S4). The -NO bond is mostly related to the organic nitrates ($RONO_2$), and the -NO_2 peak could result from both organic nitrates and nitro-organics (Bruns et al., 2010). There is no discernable peak for organic amines. These all consistently imply that the OOA2 factor contained a substantial fraction of nitrogen-containing organics, and these compounds have contributed to the absorption of secondary BrC.

3.4 Simultaneous whitening and darkening process of BrC

The relative contribution and diurnal variations of primary and secondary BrC measured by MA200 at 470, 528 and 635 nm wavelengths are similar to those at the 375 nm wavelength but with a decreased fraction of BrC absorption with increased wavelength. The mean AAE of total BrC, primary BrC and secondary BrC is obtained by power fitting on the mean absorption coefficient during the experiment (Fig. S7), which is 6.16, 5.69 and 6.40, respectively. This is consistent with other studies that SOA usually had a higher AAE than POA (Gilardoni et al., 2016; Jiang et al., 2022). Due to the high contribution of BC to total absorption ($> 50\,\%$ even at shortest wavelength), the spectral dependence of absorption in bulk has not shown apparent diurnal variation. The diurnal variation of $\sigma_{abs,375}$ for BC and primary BrC and their fractions showed consistent morning rush hour peaks at 06:00–08:00 (UTC+8) and a nighttime enhancement due to a reduced boundary layer (Fig. 4a–b). This was in line with the morning peak of HOA and night peak of BBOA. The traffic source in this region, in particular the diesel vehicles, was reported to emit considerable OA with certain chromophores, such as aromatics (Yao et al., 2015) and heterocyclic organic compounds (Gentner et al., 2017; Schuetzle, 1983). In the morning rush hour, BC and primary BrC accounted for $51 \pm 4\,\%$ and $29 \pm 4\,\%$ in the total $\sigma_{abs,375}$, respectively, with the remaining $20 \pm 2\,\%$ classified as secondary BrC. The morning peak coinciding with the primary BrC may result from the rapid formation of BrC from sources when emitted gases condensed and formed aerosols. These may lead to a high co-occurrence between primary and secondary BrC. Previous studies in urban environments also observed concurrent peaks of primary and secondary BrC, which usually occurred at morning rush hour (Zhang et al., 2020). Furthermore, the assumption of the method used to apportion primary and secondary BrC will cause some error in the distinction of the absorption coefficient; it is possible that some of the primary sources are being attributed to secondary sources and vice versa. This may be a possible reason for the simultaneous peak observed for primary and secondary BrC during morning rush hour. The night had contributions from BC and primary BrC at $50 \pm 2\,\%$ and $30 \pm 3\,\%$, respectively, with $20 \pm 3\,\%$ as secondary BrC. Figure 4b showed that the decrease of primary BrC absorption tended to be more rapid than the HOA and BBOA mass (even a slight increase for HOA, Fig. 1m and o) in the midday, leading to a decreased absorption coefficient per unit mass of primary BrC (shade in Fig. 4b), which indicates that the decrease of BrC absorptivity is likely due to photochemistry. This may involve the OH radical reaction with existing chromophores in aerosol phase (Schnitzler et al., 2020) or the enhanced evaporation of aerosols to gas phase (Palm et al., 2020) leading to further decrease of BrC absorptivity during midday. In addition to photobleaching, it is possible that some primary species transformed into less absorbing secondary BrC species. During this period, the type of HOA or BBOA that contribute to absorption may also have a lower absorptivity. In this context, a recent chamber study reported that the primary BrC from biomass burning plumes could be bleached to half of the initial absorptivity in 2–3 h (Liu et al., 2021). The reaction of BrC with OH radicals has been widely recognized as the main pathway for the loss of primary BrC absorptivity (Liu et al., 2020) and was parameterized as an exponential decrease with time at a certain OH radical concentration on a global scale (X. Wang et al., 2018).

The night and morning peak of OOA2 and the morning peak of the absorption coefficient of secondary BrC ($\sigma_{abs,secBrC}$) may result from primarily emitted moderately oxygenated OA, which was reported from some diesel sources (DeWitt et al., 2015; Gentner et al., 2012). Besides the morning rush hour peak, there was an early afternoon peak for $\sigma_{abs,secBrC}$ prevailing over the dilution effect of the daytime boundary layer (Figs. 4c and S5). The fraction of $\sigma_{abs,secBrC}$ in total σ_{abs} thus had a pronounced early afternoon peak soon after the peak solar radiation (Fig. 4f) and a peak after midnight soon after the nighttime peak of primary BrC (Fig. 4e).

Figure 4b–c showed that the MAC of POA decreased after the morning peak, but the MAC of SOA had an afternoon peak. This indicated the enhancement of absorptivity of secondary BrC, which occurred within a few hours after the peak solar radiation. These results implied that the photochemical processes decreased the absorptivity of POA but increased for that of SOA. Figure 4e–f showed the photochemical processes that led to an enhanced contribution of secondary BrC to the total absorption by 30 % from the morning rush hour to midday but during the same time reduced the contribution of primary BrC to the total absorption by about 20 %. Though other processes such as aqueous-phase reactions may cause changes to the MAC of BrC at nighttime, the apparent change in aerosol absorption observed in this study can play an im-

Table 1. Results of the multilinear regression analysis (MLR) between $\sigma_{abs,375}$ and the five PMF-resolved OA factors, with $\sigma_{abs,375}$ of total BrC, primary and secondary BrC as dependent, respectively. All regression coefficients have passed the significance test with $p < 0.01$. Partial correlations above 0.4 are marked in bold. Since negative values appear when the COA participates, which is thus not included in the final regression, the values using COA factor are shown in brackets.

Dependent	$\sigma_{abs,BrC}$		$\sigma_{abs,priBrC}$		$\sigma_{abs,secBrC}$	
Model	Regression coefficient	Partial correlation	Regression coefficient	Partial correlation	Regression coefficient	Partial correlation
Constant	2.26		1.67		1.47 (1.52)	
OOA1	0.57	0.23	0.04	0.02	0.46(0.46)	0.24 (0.24)
OOA2	1.22	**0.53**	0.37	0.25	0.74 (0.74)	**0.44 (0.44)**
BBOA	2.59	**0.46**	1.22	**0.40**	1.14 (1.18)	0.29 (0.29)
COA	1.30	0.22	1.45	0.36	– (−0.25)	– (−0.05)
HOA	1.70	**0.47**	1.17	**0.46**	0.49 (0.52)	0.20 (0.21)
R^2	0.77		0.63		0.55 (0.55)	

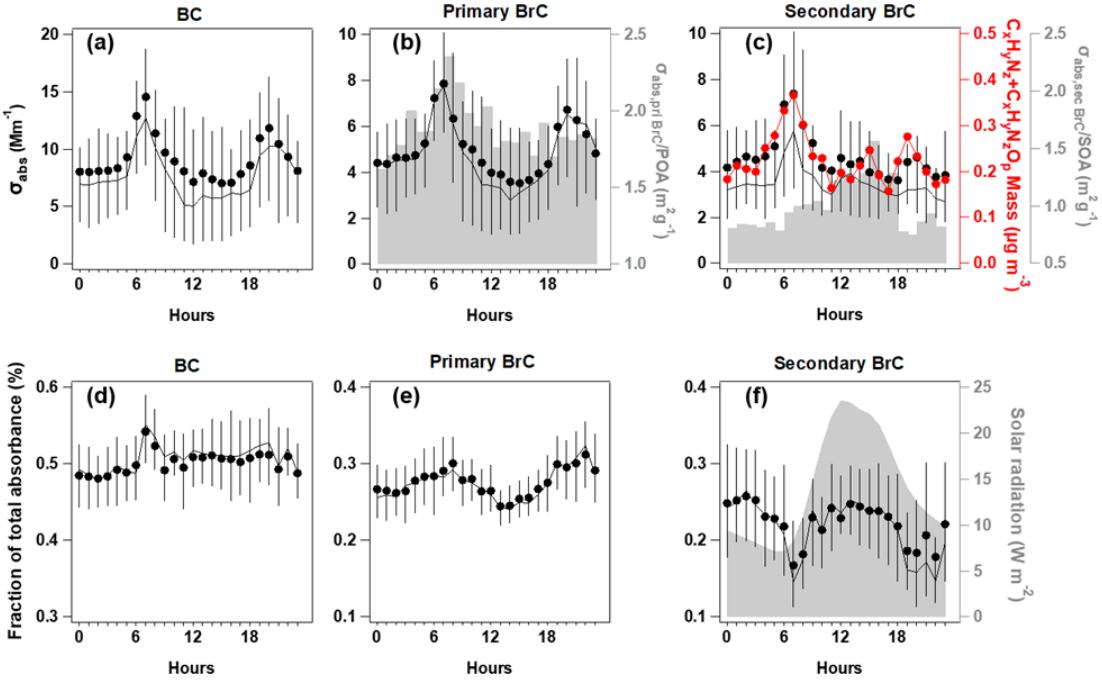

Figure 4. Diurnal variations of absorption coefficient at $\lambda = 375$ nm ($\sigma_{abs,375}$) for BC **(a)**; primary BrC and absorption efficiency of primary BrC ($\sigma_{abs,priBrC}$) / POA is shown in shading **(b)**, secondary BrC and absorption efficiency of secondary BrC ($\sigma_{abs,secBrC}$) / SOA is shown in shading, along with the $C_xH_yN_z$ and $C_xH_yN_zO_p$ fragments **(c)**; and the respective fraction in total for the segregated $\sigma_{abs,375}$ **(d–f)**, with direct radiation shown in shade. In each plot, the lines, dots and whiskers denote the median, mean and 25th/75th percentiles at each hour, respectively.

portant role in the radiative impacts due to intensive solar radiation during daytime.

Table 1 showed that the SOA compounds containing nitrogen (i.e., the OOA2) considerably contributed to the light absorption. The shift of peaking time from primary to secondary BrC demonstrates the possible processes of SOA formation, such as from gases. This aging or oxidation likely occurred through photochemical processes during early afternoon and aqueous processes (high RH conditions) during nighttime. The oxidized volatile organic compounds (VOCs) with nitrogen chemistry involved could condense to produce additional mass in the particle phase (Ehn et al., 2014; Finewax et al., 2018). The high NO_x emission of traffic VOCs may have largely involved nitrogen chemistry in the photochemical processes. Previous studies found the NO_x-involved SOA could produce considerable chromophores containing nitro-aromatics in hours (Y. Wang et al., 2019; Keyte et al., 2016). The daytime formation of organic nitrate

may follow the gas-phase photochemical processes in which the excess NO could add to the peroxy radical to produce organic nitrate (Liebmann et al., 2019). The nighttime chemistry involves an NO_3 radical through the oxidation of NO_2 by O_3, through which the organic nitrate could be produced by initializing the production of nitrooxy peroxy radicals (Ng et al., 2008; Rollins et al., 2012). Laboratory studies also widely observed the rapid production of nitrogen-containing OA through NO_x chemistry, which could contribute to light absorption of aerosols (Nakayama et al., 2013; P. F. Liu et al., 2015).

4 Conclusion

This study apportioned the shortwave absorption of BC, primary BrC and secondary BrC through concurrent measurements of BC microphysical properties and OA mass spectra. The apportioned primary BrC absorption was linked with traffic and biomass burning emissions. Primary OA generally had a higher MAC than secondary OA. OA from biomass burning was found to have the highest MAC in POA factors. Secondary BrC was found to be associated with an oxygenated secondary OA factor with higher nitrogen content. We found that the photochemical processes decreased the MAC of POA but increased the MAC of SOA, resulting in an enhanced contribution of secondary BrC to total absorbance by 30 % but a reduced contribution of primary BrC by about 20 % in the semi-urban environment. This revealed that the whitening and darkening of BrC occurred simultaneously, and the secondary BrC produced by photochemical processes may compensate for some bleaching effect of primary BrC. The dominance of both competing processes may depend on the timescale and altitude in the atmosphere. For example, the enhanced BrC fraction observed above the planetary boundary layer may be explained by the enhanced secondary BrC (Tian et al., 2020), while further aging may bleach the produced chromophores of these SOA.

The results emphasize the importance of nitrogen-containing OA in contributing to BrC. The NO_x-involved chemistry is prone to add a nitrogen element to the existing OA and enhance the absorptivity of chromophores. The anthropogenic NO_x emission could therefore be an important source in producing shortwave absorbing components in the atmosphere, which may offset some of the conventionally thought photobleaching of BrC by photochemistry. The production of secondary BrC should be considered when assessing the environment and climate impacts of light-absorbing aerosols.

Data availability. The data in this study are available from the corresponding author upon request.

Supplement. The supplement related to this article is available online at: https://doi.org/10.5194/acp-23-9439-2023-supplement.

Author contributions. DL, XJ and QiL prepared and designed the observations. DL, QiL, XJ and PT initiated the field campaign and conducted the measurements. QiL, DL, PT, YW, SL and KH contributed to the data analysis. QuL, MH, RL, KB, DD, CY and SK provided technical support and assistance. QiL and DL wrote the paper. All authors read and approved the final paper.

Competing interests. At least one of the (co-)authors is a member of the editorial board of *Atmospheric Chemistry and Physics*. The peer-review process was guided by an independent editor, and the authors also have no other competing interests to declare.

Disclaimer. Publisher's note: Copernicus Publications remains neutral with regard to jurisdictional claims in published maps and institutional affiliations.

Financial support. This research was supported by the National Natural Science Foundation of China (grant no. 42175116) and the National Key R&D Program of China (grant no. 2019YFC0214703).

Review statement. This paper was edited by Alex Lee and reviewed by three anonymous referees.

References

Aiken, A. C., Salcedo, D., Cubison, M. J., Huffman, J. A., DeCarlo, P. F., Ulbrich, I. M., Docherty, K. S., Sueper, D., Kimmel, J. R., Worsnop, D. R., Trimborn, A., Northway, M., Stone, E. A., Schauer, J. J., Volkamer, R. M., Fortner, E., de Foy, B., Wang, J., Laskin, A., Shutthanandan, V., Zheng, J., Zhang, R., Gaffney, J., Marley, N. A., Paredes-Miranda, G., Arnott, W. P., Molina, L. T., Sosa, G., and Jimenez, J. L.: Mexico City aerosol analysis during MILAGRO using high resolution aerosol mass spectrometry at the urban supersite (T0) – Part 1: Fine particle composition and organic source apportionment, Atmos. Chem. Phys., 9, 6633–6653, https://doi.org/10.5194/acp-9-6633-2009, 2009.

Andreae, M. O. and Crutzen, P. J.: Atmospheric aerosols: Biogeochemical sources and role in atmospheric chemistry, Science, 276, 1052–1058, https://doi.org/10.1126/science.276.5315.1052, 1997.

Bahadur, R., Praveen, P. S., Xu, Y., and Ramanathan, V.: Solar absorption by elemental and brown carbon determined from spectral observations, P. Natl. Acad. Sci. USA, 109, 17366–17371, https://doi.org/10.1073/pnas.1205910109, 2012.

Bond, T. C.: Spectral dependence of visible light absorption by carbonaceous particles emitted from coal combustion, Geophys. Res. Lett., 28, 4075–4078, https://doi.org/10.1029/2001gl013652, 2001.

Bond, T. C. and Bergstrom, R. W.: Light absorption by carbonaceous particles: An investigative review, Aerosol Sci. Tech., 40, 27–67, https://doi.org/10.1080/02786820500421521, 2006.

Brown, S. G., Lee, T., Roberts, P. T., and Collett, J. L., Jr.: Wintertime Residential Biomass Burning in Las Vegas, Nevada; Marker Components and Apportionment Methods, Atmosphere, 7, 58, https://doi.org/10.3390/atmos7040058, 2016.

Bruns, E. A., Perraud, V., Zelenyuk, A., Ezell, M. J., Johnson, S. N., Yu, Y., Imre, D., Finlayson-Pitts, B. J., and Alexander, M. L.: Comparison of FTIR and Particle Mass Spectrometry for the Measurement of Particulate Organic Nitrates, Environ. Sci. Technol., 44, 1056–1061, https://doi.org/10.1021/es9029864, 2010.

Canagaratna, M. R., Jayne, J. T., Jimenez, J. L., Allan, J. D., Alfarra, M. R., Zhang, Q., Onasch, T. B., Drewnick, F., Coe, H., Middlebrook, A., Delia, A., Williams, L. R., Trimborn, A. M., Northway, M. J., DeCarlo, P. F., Kolb, C. E., Davidovits, P., and Worsnop, D. R.: Chemical and microphysical characterization of ambient aerosols with the aerodyne aerosol mass spectrometer, Mass Spectrom. Rev., 26, 185–222, https://doi.org/10.1002/mas.20115, 2007.

Canagaratna, M. R., Jimenez, J. L., Kroll, J. H., Chen, Q., Kessler, S. H., Massoli, P., Hildebrandt Ruiz, L., Fortner, E., Williams, L. R., Wilson, K. R., Surratt, J. D., Donahue, N. M., Jayne, J. T., and Worsnop, D. R.: Elemental ratio measurements of organic compounds using aerosol mass spectrometry: characterization, improved calibration, and implications, Atmos. Chem. Phys., 15, 253–272, https://doi.org/10.5194/acp-15-253-2015, 2015.

Cheng, Y., Engling, G., He, K.-B., Duan, F.-K., Ma, Y.-L., Du, Z.-Y., Liu, J.-M., Zheng, M., and Weber, R. J.: Biomass burning contribution to Beijing aerosol, Atmos. Chem. Phys., 13, 7765–7781, https://doi.org/10.5194/acp-13-7765-2013, 2013.

Coury, C. and Dillner, A. M.: A method to quantify organic functional groups and inorganic compounds in ambient aerosols using attenuated total reflectance FTIR spectroscopy and multivariate chemometric techniques, Atmos. Environ., 42, 5923–5932, https://doi.org/10.1016/j.atmosenv.2008.03.026, 2008.

Crilley, L. R., Bloss, W. J., Yin, J., Beddows, D. C. S., Harrison, R. M., Allan, J. D., Young, D. E., Flynn, M., Williams, P., Zotter, P., Prevot, A. S. H., Heal, M. R., Barlow, J. F., Halios, C. H., Lee, J. D., Szidat, S., and Mohr, C.: Sources and contributions of wood smoke during winter in London: assessing local and regional influences, Atmos. Chem. Phys., 15, 3149–3171, https://doi.org/10.5194/acp-15-3149-2015, 2015.

Cubison, M. J., Ortega, A. M., Hayes, P. L., Farmer, D. K., Day, D., Lechner, M. J., Brune, W. H., Apel, E., Diskin, G. S., Fisher, J. A., Fuelberg, H. E., Hecobian, A., Knapp, D. J., Mikoviny, T., Riemer, D., Sachse, G. W., Sessions, W., Weber, R. J., Weinheimer, A. J., Wisthaler, A., and Jimenez, J. L.: Effects of aging on organic aerosol from open biomass burning smoke in aircraft and laboratory studies, Atmos. Chem. Phys., 11, 12049–12064, https://doi.org/10.5194/acp-11-12049-2011, 2011.

Dasari, S., Andersson, A., Bikkina, S., Holmstrand, H., Budhavant, K., Satheesh, S., Asmi, E., Kesti, J., Backman, J., Salam, A., Bisht, D. S., Tiwari, S., Hameed, Z., and Gustafsson, O.: Photochemical degradation affects the light absorption of water-soluble brown carbon in the South Asian outflow, Science Advances, 5, eaau8066, https://doi.org/10.1126/sciadv.aau8066, 2019.

DeCarlo, P. F., Ulbrich, I. M., Crounse, J., de Foy, B., Dunlea, E. J., Aiken, A. C., Knapp, D., Weinheimer, A. J., Campos, T., Wennberg, P. O., and Jimenez, J. L.: Investigation of the sources and processing of organic aerosol over the Central Mexican Plateau from aircraft measurements during MILAGRO, Atmos. Chem. Phys., 10, 5257–5280, https://doi.org/10.5194/acp-10-5257-2010, 2010.

DeWitt, H. L., Hellebust, S., Temime-Roussel, B., Ravier, S., Polo, L., Jacob, V., Buisson, C., Charron, A., André, M., Pasquier, A., Besombes, J. L., Jaffrezo, J. L., Wortham, H., and Marchand, N.: Near-highway aerosol and gas-phase measurements in a high-diesel environment, Atmos. Chem. Phys., 15, 4373–4387, https://doi.org/10.5194/acp-15-4373-2015, 2015.

Ding, S., Liu, D., Zhao, D., Hu, K., Tian, P., Zhou, W., Huang, M., Yang, Y., Wang, F., Sheng, J., Liu, Q., Kong, S., Cui, P., Huang, Y., He, H., Coe, H., and Ding, D.: Size-Related Physical Properties of Black Carbon in the Lower Atmosphere over Beijing and Europe, Environ. Sci. Technol., 53, 11112–11121, https://doi.org/10.1021/acs.est.9b03722, 2019.

Draxier, R. R. and Hess, G. D.: An overview of the HYSPLIT_4 modelling system for trajectories, dispersion and deposition, Aust. Meteorol. Mag., 47, 295–308, 1998.

Drinovec, L., Močnik, G., Zotter, P., Prévôt, A. S. H., Ruckstuhl, C., Coz, E., Rupakheti, M., Sciare, J., Müller, T., Wiedensohler, A., and Hansen, A. D. A.: The "dual-spot" Aethalometer: an improved measurement of aerosol black carbon with real-time loading compensation, Atmos. Meas. Tech., 8, 1965–1979, https://doi.org/10.5194/amt-8-1965-2015, 2015.

Düsing, S., Wehner, B., Müller, T., Stöcker, A., and Wiedensohler, A.: The effect of rapid relative humidity changes on fast filter-based aerosol-particle light-absorption measurements: uncertainties and correction schemes, Atmos. Meas. Tech., 12, 5879–5895, https://doi.org/10.5194/amt-12-5879-2019, 2019.

Ehn, M., Thornton, J. A., Kleist, E., Sipila, M., Junninen, H., Pullinen, I., Springer, M., Rubach, F., Tillmann, R., Lee, B., Lopez-Hilfiker, F., Andres, S., Acir, I.-H., Rissanen, M., Jokinen, T., Schobesberger, S., Kangasluoma, J., Kontkanen, J., Nieminen, T., Kurten, T., Nielsen, L. B., Jorgensen, S., Kjaergaard, H. G., Canagaratna, M., Dal Maso, M., Berndt, T., Petaja, T., Wahner, A., Kerminen, V.-M., Kulmala, M., Worsnop, D. R., Wildt, J., and Mentel, T. F.: A large source of low-volatility secondary organic aerosol, Nature, 506, 476–479, https://doi.org/10.1038/nature13032, 2014.

Elser, M., Huang, R.-J., Wolf, R., Slowik, J. G., Wang, Q., Canonaco, F., Li, G., Bozzetti, C., Daellenbach, K. R., Huang, Y., Zhang, R., Li, Z., Cao, J., Baltensperger, U., El-Haddad, I., and Prévôt, A. S. H.: New insights into $PM_{2.5}$ chemical composition and sources in two major cities in China during extreme haze events using aerosol mass spectrometry, Atmos. Chem. Phys., 16, 3207–3225, https://doi.org/10.5194/acp-16-3207-2016, 2016.

Finewax, Z., de Gouw, J. A., and Ziemann, P. J.: Identification and Quantification of 4-Nitrocatechol Formed from OH and NO_3 Radical-Initiated Reactions of Catechol in Air in the Presence of NO_x: Implications for Secondary Organic Aerosol Formation from Biomass Burning, Environ. Sci. Technol., 52, 1981–1989, https://doi.org/10.1021/acs.est.7b05864, 2018.

Forrister, H., Liu, J., Scheuer, E., Dibb, J., Ziemba, L., Thornhill, K. L., Anderson, B., Diskin, G., Perring, A. E., Schwarz, J. P., Campuzano-Jost, P., Day, D. A., Palm, B. B., Jimenez,

J. L., Nenes, A., and Weber, R. J.: Evolution of brown carbon in wildfire plumes, Geophys. Res. Lett., 42, 4623–4630, https://doi.org/10.1002/2015gl063897, 2015.

Gao, Y., Wang, Q., Li, L., Dai, W., Yu, J., Ding, L., Li, J., Xin, B., Ran, W., Han, Y., and Cao, J.: Optical properties of mountain primary and secondary brown carbon aerosols in summertime, Sci. Total Environ., 806, 150570, https://doi.org/10.1016/j.scitotenv.2021.150570, 2022.

Gentner, D. R., Isaacman, G., Worton, D. R., Chan, A. W. H., Dallmann, T. R., Davis, L., Liu, S., Day, D. A., Russell, L. M., Wilson, K. R., Weber, R., Guha, A., Harley, R. A., and Goldstein, A. H.: Elucidating secondary organic aerosol from diesel and gasoline vehicles through detailed characterization of organic carbon emissions, P. Natl. Acad. Sci. USA, 109, 18318–18323, https://doi.org/10.1073/pnas.1212272109, 2012.

Gentner, D. R., Jathar, S. H., Gordon, T. D., Bahreini, R., Day, D. A., El Haddad, I., Hayes, P. L., Pieber, S. M., Platt, S. M., de Gouw, J., Goldstein, A. H., Harley, R. A., Jimenez, J. L., Prevot, A. S. H., and Robinson, A. L.: Review of Urban Secondary Organic Aerosol Formation from Gasoline and Diesel Motor Vehicle Emissions, Environ. Sci. Technol., 51, 1074–1093, https://doi.org/10.1021/acs.est.6b04509, 2017.

Gilardoni, S., Massoli, P., Paglione, M., Giulianelli, L., Carbone, C., Rinaldi, M., Decesari, S., Sandrini, S., Costabile, F., Gobbi, G. P., Pietrogrande, M. C., Visentin, M., Scotto, F., Fuzzi, S., and Facchini, M. C.: Direct observation of aqueous secondary organic aerosol from biomass-burning emissions, P. Natl. Acad. Sci. USA, 113, 10013–10018, https://doi.org/10.1073/pnas.1602212113, 2016.

Hayes, P. L., Ortega, A. M., Cubison, M. J., Froyd, K. D., Zhao, Y., Cliff, S. S., Hu, W. W., Toohey, D. W., Flynn, J. H., Lefer, B. L., Grossberg, N., Alvarez, S., Rappenglueck, B., Taylor, J. W., Allan, J. D., Holloway, J. S., Gilman, J. B., Kuster, W. C., De Gouw, J. A., Massoli, P., Zhang, X., Liu, J., Weber, R. J., Corrigan, A. L., Russell, L. M., Isaacman, G., Worton, D. R., Kreisberg, N. M., Goldstein, A. H., Thalman, R., Waxman, E. M., Volkamer, R., Lin, Y. H., Surratt, J. D., Kleindienst, T. E., Offenberg, J. H., Dusanter, S., Griffith, S., Stevens, P. S., Brioude, J., Angevine, W. M., and Jimenez, J. L.: Organic aerosol composition and sources in Pasadena, California, during the 2010 CalNex campaign, J. Geophys. Res.-Atmos., 118, 9233–9257, https://doi.org/10.1002/jgrd.50530, 2013.

Hu, K., Liu, D., Tian, P., Wu, Y., Deng, Z., Wu, Y., Zhao, D., Li, R., Sheng, J., Huang, M., Ding, D., Li, W., Wang, Y., and Wu, Y.: Measurements of the Diversity of Shape and Mixing State for Ambient Black Carbon Particles, Geophys. Res. Lett., 48, e2021GL094522, https://doi.org/10.1029/2021GL094522, 2021.

Hu, W., Hu, M., Hu, W.-W., Zheng, J., Chen, C., Wu, Y., and Guo, S.: Seasonal variations in high time-resolved chemical compositions, sources, and evolution of atmospheric submicron aerosols in the megacity Beijing, Atmos. Chem. Phys., 17, 9979–10000, https://doi.org/10.5194/acp-17-9979-2017, 2017.

Huang, D. D., Zhu, S., An, J., Wang, Q., Qiao, L., Zhou, M., He, X., Ma, Y., Sun, Y., Huang, C., Yu, J. Z., and Zhang, Q.: Comparative Assessment of Cooking Emission Contributions to Urban Organic Aerosol Using Online Molecular Tracers and Aerosol Mass Spectrometry Measurements, Environ. Sci. Technol., 55, 14526–14535, https://doi.org/10.1021/acs.est.1c03280, 2021.

Huffman, J. A., Docherty, K. S., Aiken, A. C., Cubison, M. J., Ulbrich, I. M., DeCarlo, P. F., Sueper, D., Jayne, J. T., Worsnop, D. R., Ziemann, P. J., and Jimenez, J. L.: Chemically-resolved aerosol volatility measurements from two megacity field studies, Atmos. Chem. Phys., 9, 7161–7182, https://doi.org/10.5194/acp-9-7161-2009, 2009.

Jacobson, M. Z.: Isolating nitrated and aromatic aerosols and nitrated aromatic gases as sources of ultraviolet light absorption, J. Geophys. Res.-Atmos., 104, 3527–3542, https://doi.org/10.1029/1998jd100054, 1999.

Jayne, J. T., Leard, D. C., Zhang, X. F., Davidovits, P., Smith, K. A., Kolb, C. E., and Worsnop, D. R.: Development of an aerosol mass spectrometer for size and composition analysis of submicron particles, Aerosol Sci. Tech., 33, 49–70, https://doi.org/10.1080/027868200410840, 2000.

Jiang, X., Liu, D., Li, Q., Tian, P., Wu, Y., Li, S., Hu, K., Ding, S., Bi, K., Li, R., Huang, M., Ding, D., Chen, Q., Kong, S., Li, W., Pang, Y., and He, D.: Connecting the Light Absorption of Atmospheric Organic Aerosols with Oxidation State and Polarity, Environ. Sci. Technol., 56, 12873–12885, https://doi.org/10.1021/acs.est.2c02202, 2022.

Jimenez, J. L., Canagaratna, M. R., Donahue, N. M., Prevot, A. S. H., Zhang, Q., Kroll, J. H., DeCarlo, P. F., Allan, J. D., Coe, H., Ng, N. L., Aiken, A. C., Docherty, K. S., Ulbrich, I. M., Grieshop, A. P., Robinson, A. L., Duplissy, J., Smith, J. D., Wilson, K. R., Lanz, V. A., Hueglin, C., Sun, Y. L., Tian, J., Laaksonen, A., Raatikainen, T., Rautiainen, J., Vaattovaara, P., Ehn, M., Kulmala, M., Tomlinson, J. M., Collins, D. R., Cubison, M. J., Dunlea, E. J., Huffman, J. A., Onasch, T. B., Alfarra, M. R., Williams, P. I., Bower, K., Kondo, Y., Schneider, J., Drewnick, F., Borrmann, S., Weimer, S., Demerjian, K., Salcedo, D., Cottrell, L., Griffin, R., Takami, A., Miyoshi, T., Hatakeyama, S., Shimono, A., Sun, J. Y., Zhang, Y. M., Dzepina, K., Kimmel, J. R., Sueper, D., Jayne, J. T., Herndon, S. C., Trimborn, A. M., Williams, L. R., Wood, E. C., Middlebrook, A. M., Kolb, C. E., Baltensperger, U., and Worsnop, D. R.: Evolution of Organic Aerosols in the Atmosphere, Science, 326, 1525–1529, https://doi.org/10.1126/science.1180353, 2009.

Kasthuriarachchi, N. Y., Rivellini, L.-H., Adam, M. G., and Lee, A. K. Y.: Light Absorbing Properties of Primary and Secondary Brown Carbon in a Tropical Urban Environment, Environ. Sci. Technol., 54, 10808–10819, https://doi.org/10.1021/acs.est.0c02414, 2020.

Keyte, I. J., Albinet, A., and Harrison, R. M.: On-road traffic emissions of polycyclic aromatic hydrocarbons and their oxy- and nitro-derivative compounds measured in road tunnel environments, Sci. Total Environ., 566, 1131–1142, https://doi.org/10.1016/j.scitotenv.2016.05.152, 2016.

Laborde, M., Schnaiter, M., Linke, C., Saathoff, H., Naumann, K.-H., Möhler, O., Berlenz, S., Wagner, U., Taylor, J. W., Liu, D., Flynn, M., Allan, J. D., Coe, H., Heimerl, K., Dahlkötter, F., Weinzierl, B., Wollny, A. G., Zanatta, M., Cozic, J., Laj, P., Hitzenberger, R., Schwarz, J. P., and Gysel, M.: Single Particle Soot Photometer intercomparison at the AIDA chamber, Atmos. Meas. Tech., 5, 3077–3097, https://doi.org/10.5194/amt-5-3077-2012, 2012.

Laskin, A., Laskin, J., and Nizkorodov, S. A.: Chemistry of Atmospheric Brown Carbon, Chem. Rev., 115, 4335–4382, https://doi.org/10.1021/cr5006167, 2015.

Liebmann, J., Sobanski, N., Schuladen, J., Karu, E., Hellén, H., Hakola, H., Zha, Q., Ehn, M., Riva, M., Heikkinen, L., Williams, J., Fischer, H., Lelieveld, J., and Crowley, J. N.: Alkyl nitrates in the boreal forest: formation via the NO3-, OH- and O3-induced oxidation of biogenic volatile organic compounds and ambient lifetimes, Atmos. Chem. Phys., 19, 10391–10403, https://doi.org/10.5194/acp-19-10391-2019, 2019.

Liu, D., Allan, J. D., Young, D. E., Coe, H., Beddows, D., Fleming, Z. L., Flynn, M. J., Gallagher, M. W., Harrison, R. M., Lee, J., Prevot, A. S. H., Taylor, J. W., Yin, J., Williams, P. I., and Zotter, P.: Size distribution, mixing state and source apportionment of black carbon aerosol in London during wintertime, Atmos. Chem. Phys., 14, 10061–10084, https://doi.org/10.5194/acp-14-10061-2014, 2014.

Liu, D., Taylor, J. W., Young, D. E., Flynn, M. J., Coe, H., and Allan, J. D.: The effect of complex black carbon microphysics on the determination of the optical properties of brown carbon, Geophys. Res. Lett., 42, 613–619, https://doi.org/10.1002/2014gl062443, 2015.

Liu, D., Joshi, R., Wang, J., Yu, C., Allan, J. D., Coe, H., Flynn, M. J., Xie, C., Lee, J., Squires, F., Kotthaus, S., Grimmond, S., Ge, X., Sun, Y., and Fu, P.: Contrasting physical properties of black carbon in urban Beijing between winter and summer, Atmos. Chem. Phys., 19, 6749–6769, https://doi.org/10.5194/acp-19-6749-2019, 2019.

Liu, D., He, C., Schwarz, J. P., and Wang, X.: Lifecycle of light-absorbing carbonaceous aerosols in the atmosphere, npj Clim. Atmos. Sci., 3, 40, https://doi.org/10.1038/s41612-020-00145-8, 2020.

Liu, D., Li, S., Hu, D., Kong, S., Cheng, Y., Wu, Y., Ding, S., Hu, K., Zheng, S., Yan, Q., Zheng, H., Zhao, D., Tian, P., Ye, J., Huang, M., and Ding, D.: Evolution of Aerosol Optical Properties from Wood Smoke in Real Atmosphere Influenced by Burning Phase and Solar Radiation, Environ. Sci. Technol., 55, 5677–5688, https://doi.org/10.1021/acs.est.0c07569, 2021.

Liu, F., Zhang, Q., Tong, D., Zheng, B., Li, M., Huo, H., and He, K. B.: High-resolution inventory of technologies, activities, and emissions of coal-fired power plants in China from 1990 to 2010, Atmos. Chem. Phys., 15, 13299–13317, https://doi.org/10.5194/acp-15-13299-2015, 2015.

Liu, J., Mauzerall, D. L., Chen, Q., Zhang, Q., Song, Y., Peng, W., Klimont, Z., Qiu, X., Zhang, S., Hu, M., Lin, W., Smith, K. R., and Zhu, T.: Air pollutant emissions from Chinese households: A major and underappreciated ambient pollution source, P. Natl. Acad. Sci. USA, 113, 7756–7761, https://doi.org/10.1073/pnas.1604537113, 2016.

Liu, P. F., Abdelmalki, N., Hung, H.-M., Wang, Y., Brune, W. H., and Martin, S. T.: Ultraviolet and visible complex refractive indices of secondary organic material produced by photooxidation of the aromatic compounds toluene and m-xylene, Atmos. Chem. Phys., 15, 1435–1446, https://doi.org/10.5194/acp-15-1435-2015, 2015.

Makra, L., Matyasovszky, I., Guba, Z., Karatzas, K., and Anttila, P.: Monitoring the long-range transport effects on urban PM_{10} levels using 3D clusters of backward trajectories, Atmos. Environ., 45, 2630–2641, https://doi.org/10.1016/j.atmosenv.2011.02.068, 2011.

Middlebrook, A. M., Bahreini, R., Jimenez, J. L., and Canagaratna, M. R.: Evaluation of Composition-Dependent Collection Efficiencies for the Aerodyne Aerosol Mass Spectrometer using Field Data, Aerosol Sci. Tech., 46, 258–271, https://doi.org/10.1080/02786826.2011.620041, 2012.

Mohr, C., DeCarlo, P. F., Heringa, M. F., Chirico, R., Slowik, J. G., Richter, R., Reche, C., Alastuey, A., Querol, X., Seco, R., Peñuelas, J., Jiménez, J. L., Crippa, M., Zimmermann, R., Baltensperger, U., and Prévôt, A. S. H.: Identification and quantification of organic aerosol from cooking and other sources in Barcelona using aerosol mass spectrometer data, Atmos. Chem. Phys., 12, 1649–1665, https://doi.org/10.5194/acp-12-1649-2012, 2012.

Nakayama, T., Sato, K., Matsumi, Y., Imamura, T., Yamazaki, A., and Uchiyama, A.: Wavelength and NO_x dependent complex refractive index of SOAs generated from the photooxidation of toluene, Atmos. Chem. Phys., 13, 531–545, https://doi.org/10.5194/acp-13-531-2013, 2013.

Ng, N. L., Kwan, A. J., Surratt, J. D., Chan, A. W. H., Chhabra, P. S., Sorooshian, A., Pye, H. O. T., Crounse, J. D., Wennberg, P. O., Flagan, R. C., and Seinfeld, J. H.: Secondary organic aerosol (SOA) formation from reaction of isoprene with nitrate radicals (NO_3), Atmos. Chem. Phys., 8, 4117–4140, https://doi.org/10.5194/acp-8-4117-2008, 2008.

Paatero, P. and Tapper, U.: Positive Matrix Factorization – A Nonnegative Factor Model With Optimal Utilization Of Error-Estimates Of Data Values, Environmetrics, 5, 111–126, https://doi.org/10.1002/env.3170050203, 1994.

Pachon, J. E., Weber, R. J., Zhang, X., Mulholland, J. A., and Russell, A. G.: Revising the use of potassium (K) in the source apportionment of $PM_{2.5}$, Atmos. Pollut. Res., 4, 14–21, https://doi.org/10.5094/apr.2013.002, 2013.

Palm, B. B., Peng, Q., Fredrickson, C. D., Lee, B. H., Garofalo, L. A., Pothier, M. A., Kreidenweis, S. M., Farmer, D. K., Pokhrel, R. P., Shen, Y., Murphy, S. M., Permar, W., Hu, L., Campos, T. L., Hall, S. R., Ullmann, K., Zhang, X., Flocke, F., Fischer, E. V., and Thornton, J. A.: Quantification of organic aerosol and brown carbon evolution in fresh wildfire plumes, P. Natl. Acad. Sci. USA, 117, 29469–29477, https://doi.org/10.1073/pnas.2012218117, 2020.

Qin, Y. M., Tan, H. B., Li, Y. J., Li, Z. J., Schurman, M. I., Liu, L., Wu, C., and Chan, C. K.: Chemical characteristics of brown carbon in atmospheric particles at a suburban site near Guangzhou, China, Atmos. Chem. Phys., 18, 16409–16418, https://doi.org/10.5194/acp-18-16409-2018, 2018.

Rizzo, L. V., Artaxo, P., Müller, T., Wiedensohler, A., Paixão, M., Cirino, G. G., Arana, A., Swietlicki, E., Roldin, P., Fors, E. O., Wiedemann, K. T., Leal, L. S. M., and Kulmala, M.: Long term measurements of aerosol optical properties at a primary forest site in Amazonia, Atmos. Chem. Phys., 13, 2391–2413, https://doi.org/10.5194/acp-13-2391-2013, 2013.

Rollins, A. W., Browne, E. C., Min, K. E., Pusede, S. E., Wooldridge, P. J., Gentner, D. R., Goldstein, A. H., Liu, S., Day, D. A., Russell, L. M., and Cohen, R. C.: Evidence for NO_x Control over Nighttime SOA Formation, Science, 337, 1210–1212, https://doi.org/10.1126/science.1221520, 2012.

Satish, R. and Rastogi, N.: On the Use of Brown Carbon Spectra as a Tool to Understand Their Broader Composition and Characteristics: A Case Study from Crop-residue Burning Samples, Acs Omega, 4, 1847–1853, https://doi.org/10.1021/acsomega.8b02637, 2019.

Satish, R., Shamjad, P., Thamban, N., Tripathi, S., and Rastogi, N.: Temporal Characteristics of Brown Carbon over the Central Indo-Gangetic Plain, Environ. Sci. Technol., 51, 6765–6772, https://doi.org/10.1021/acs.est.7b00734, 2017.

Schnitzler, E. G., Liu, T., Hems, R. F., and Abbatt, J. P. D.: Emerging investigator series: heterogeneous OH oxidation of primary brown carbon aerosol: effects of relative humidity and volatility, Environ. Sci.-Proc. Imp., 22, 2162–2171, https://doi.org/10.1039/d0em00311e, 2020.

Schuetzle, D.: Sampling Of Vehicle Emissions For Chemical-Analysis And Biological Testing, Environ. Health Persp., 47, 65–80, https://doi.org/10.2307/3429500, 1983.

Schwarz, J. P., Spackman, J. R., Fahey, D. W., Gao, R. S., Lohmann, U., Stier, P., Watts, L. A., Thomson, D. S., Lack, D. A., Pfister, L., Mahoney, M. J., Baumgardner, D., Wilson, J. C., and Reeves, J. M.: Coatings and their enhancement of black carbon light absorption in the tropical atmosphere, J. Geophys. Res.-Atmos., 113, D03203, https://doi.org/10.1029/2007jd009042, 2008.

Shen, G., Ru, M., Du, W., Zhu, X., Zhong, Q., Chen, Y., Shen, H., Yun, X., Meng, W., Liu, J., Cheng, H., Hu, J., Guan, D., and Tao, S.: Impacts of air pollutants from rural Chinese households under the rapid residential energy transition, Nat. Commun., 10, 3405, https://doi.org/10.1038/s41467-019-11453-w, 2019.

Sun, Y., Jiang, Q., Wang, Z., Fu, P., Li, J., Yang, T., and Yin, Y.: Investigation of the sources and evolution processes of severe haze pollution in Beijing in January 2013, J. Geophys. Res.-Atmos., 119, 4380–4398, https://doi.org/10.1002/2014jd021641, 2014.

Sun, Y., Du, W., Fu, P., Wang, Q., Li, J., Ge, X., Zhang, Q., Zhu, C., Ren, L., Xu, W., Zhao, J., Han, T., Worsnop, D. R., and Wang, Z.: Primary and secondary aerosols in Beijing in winter: sources, variations and processes, Atmos. Chem. Phys., 16, 8309–8329, https://doi.org/10.5194/acp-16-8309-2016, 2016.

Sun, Y. L., Zhang, Q., Schwab, J. J., Chen, W. N., Bae, M. S., Lin, Y. C., Hung, H. M., and Demerjian, K. L.: A case study of aerosol processing and evolution in summer in New York City, Atmos. Chem. Phys., 11, 12737–12750, https://doi.org/10.5194/acp-11-12737-2011, 2011a.

Sun, Y.-L., Zhang, Q., Schwab, J. J., Demerjian, K. L., Chen, W.-N., Bae, M.-S., Hung, H.-M., Hogrefe, O., Frank, B., Rattigan, O. V., and Lin, Y.-C.: Characterization of the sources and processes of organic and inorganic aerosols in New York city with a high-resolution time-of-flight aerosol mass apectrometer, Atmos. Chem. Phys., 11, 1581–1602, https://doi.org/10.5194/acp-11-1581-2011, 2011b.

Taylor, J. W., Allan, J. D., Liu, D., Flynn, M., Weber, R., Zhang, X., Lefer, B. L., Grossberg, N., Flynn, J., and Coe, H.: Assessment of the sensitivity of core / shell parameters derived using the single-particle soot photometer to density and refractive index, Atmos. Meas. Tech., 8, 1701–1718, https://doi.org/10.5194/amt-8-1701-2015, 2015.

Tian, P., Liu, D., Zhao, D., Yu, C., Liu, Q., Huang, M., Deng, Z., Ran, L., Wu, Y., Ding, S., Hu, K., Zhao, G., Zhao, C., and Ding, D.: In situ vertical characteristics of optical properties and heating rates of aerosol over Beijing, Atmos. Chem. Phys., 20, 2603–2622, https://doi.org/10.5194/acp-20-2603-2020, 2020.

Ulbrich, I. M., Canagaratna, M. R., Zhang, Q., Worsnop, D. R., and Jimenez, J. L.: Interpretation of organic components from Positive Matrix Factorization of aerosol mass spectrometric data, Atmos. Chem. Phys., 9, 2891–2918, https://doi.org/10.5194/acp-9-2891-2009, 2009.

Updyke, K. M., Nguyen, T. B., and Nizkorodov, S. A.: Formation of brown carbon via reactions of ammonia with secondary organic aerosols from biogenic and anthropogenic precursors, Atmos. Environ., 63, 22–31, https://doi.org/10.1016/j.atmosenv.2012.09.012, 2012.

Wang, J., Ye, J., Zhang, Q., Zhao, J., Wu, Y., Li, J., Liu, D., Li, W., Zhang, Y., Wu, C., Xie, C., Qin, Y., Lei, Y., Huang, X., Guo, J., Liu, P., Fu, P., Li, Y., Lee, H. C., Choi, H., Zhang, J., Liao, H., Chen, M., Sun, Y., Ge, X., Martin, S. T., and Jacob, D. J.: Aqueous production of secondary organic aerosol from fossil-fuel emissions in winter Beijing haze, P. Natl. Acad. Sci. USA, 118, e2022179118, https://doi.org/10.1073/pnas.2022179118, 2021.

Wang, Q., Cao, J., Han, Y., Tian, J., Zhang, Y., Pongpiachan, S., Zhang, Y., Li, L., Niu, X., Shen, Z., Zhao, Z., Tipmanee, D., Bunsomboonsakul, S., Chen, Y., and Sun, J.: Enhanced light absorption due to the mixing state of black carbon in fresh biomass burning emissions, Atmos. Environ., 180, 184–191, https://doi.org/10.1016/j.atmosenv.2018.02.049, 2018.

Wang, Q., Han, Y., Ye, J., Liu, S., Pongpiachan, S., Zhang, N., Han, Y., Tian, J., Wu, C., Long, X., Zhang, Q., Zhang, W., Zhao, Z., and Cao, J.: High Contribution of Secondary Brown Carbon to Aerosol Light Absorption in the Southeastern Margin of Tibetan Plateau, Geophys. Res. Lett., 46, 4962–4970, https://doi.org/10.1029/2019gl082731, 2019a.

Wang, Q., Ye, J., Wang, Y., Zhang, T., Ran, W., Wu, Y., Tian, J., Li, L., Zhou, Y., Hang Ho, S. S., Dang, B., Zhang, Q., Zhang, R., Chen, Y., Zhu, C., and Cao, J.: Wintertime Optical Properties of Primary and Secondary Brown Carbon at a Regional Site in the North China Plain, Environ. Sci. Technol., 53, 12389–12397, https://doi.org/10.1021/acs.est.9b03406, 2019b.

Wang, Q., Liu, H., Wang, P., Dai, W., Zhang, T., Zhao, Y., Tian, J., Zhang, W., Han, Y., and Cao, J.: Optical source apportionment and radiative effect of light-absorbing carbonaceous aerosols in a tropical marine monsoon climate zone: the importance of ship emissions, Atmos. Chem. Phys., 20, 15537–15549, https://doi.org/10.5194/acp-20-15537-2020, 2020.

Wang, X., Heald, C. L., Ridley, D. A., Schwarz, J. P., Spackman, J. R., Perring, A. E., Coe, H., Liu, D., and Clarke, A. D.: Exploiting simultaneous observational constraints on mass and absorption to estimate the global direct radiative forcing of black carbon and brown carbon, Atmos. Chem. Phys., 14, 10989–11010, https://doi.org/10.5194/acp-14-10989-2014, 2014.

Wang, X., Heald, C. L., Liu, J., Weber, R. J., Campuzano-Jost, P., Jimenez, J. L., Schwarz, J. P., and Perring, A. E.: Exploring the observational constraints on the simulation of brown carbon, Atmos. Chem. Phys., 18, 635–653, https://doi.org/10.5194/acp-18-635-2018, 2018.

Wang, Y., Hu, M., Wang, Y., Zheng, J., Shang, D., Yang, Y., Liu, Y., Li, X., Tang, R., Zhu, W., Du, Z., Wu, Y., Guo, S., Wu, Z., Lou, S., Hallquist, M., and Yu, J. Z.: The formation of nitro-aromatic compounds under high NO_x and anthropogenic VOC conditions in urban Beijing, China, Atmos. Chem. Phys., 19, 7649–7665, https://doi.org/10.5194/acp-19-7649-2019, 2019.

Wu, C. and Yu, J. Z.: Determination of primary combustion source organic carbon-to-elemental carbon (OC / EC) ratio using ambient OC and EC measurements: secondary OC-EC correla-

tion minimization method, Atmos. Chem. Phys., 16, 5453–5465, https://doi.org/10.5194/acp-16-5453-2016, 2016.

Yang, W., Zhang, Y., Wang, X., Li, S., Zhu, M., Yu, Q., Li, G., Huang, Z., Zhang, H., Wu, Z., Song, W., Tan, J., and Shao, M.: Volatile organic compounds at a rural site in Beijing: influence of temporary emission control and wintertime heating, Atmos. Chem. Phys., 18, 12663–12682, https://doi.org/10.5194/acp-18-12663-2018, 2018.

Yao, Z., Shen, X., Ye, Y., Cao, X., Jiang, X., Zhang, Y., and He, K.: On-road emission characteristics of VOCs from diesel trucks in Beijing, China, Atmos. Environ., 103, 87–93, https://doi.org/10.1016/j.atmosenv.2014.12.028, 2015.

Zhang, Q., Worsnop, D. R., Canagaratna, M. R., and Jimenez, J. L.: Hydrocarbon-like and oxygenated organic aerosols in Pittsburgh: insights into sources and processes of organic aerosols, Atmos. Chem. Phys., 5, 3289–3311, https://doi.org/10.5194/acp-5-3289-2005, 2005.

Zhang, Q., Jimenez, J. L., Canagaratna, M. R., Ulbrich, I. M., Ng, N. L., Worsnop, D. R., and Sun, Y.: Understanding atmospheric organic aerosols via factor analysis of aerosol mass spectrometry: a review, Anal. Bioanal. Chem., 401, 3045–3067, https://doi.org/10.1007/s00216-011-5355-y, 2011.

Zhang, Q., Shen, Z., Zhang, L., Zeng, Y., Ning, Z., Zhang, T., Lei, Y., Wang, Q., Li, G., Sun, J., Westerdahl, D., Xu, H., and Cao, J.: Investigation of Primary and Secondary Particulate Brown Carbon in Two Chinese Cities of Xi'an and Hong Kong in Wintertime, Environ. Sci. Technol., 54, 3803–3813, https://doi.org/10.1021/acs.est.9b05332, 2020.

Zhang, Y., Zhang, Q., Cheng, Y., Su, H., Li, H., Li, M., Zhang, X., Ding, A., and He, K.: Amplification of light absorption of black carbon associated with air pollution, Atmos. Chem. Phys., 18, 9879–9896, https://doi.org/10.5194/acp-18-9879-2018, 2018.

Zhang, Y., Wang, Q., Tian, J., Li, Y., Liu, H., Ran, W., Han, Y., Prévôt, A. S. H., and Cao, J.: Impact of COVID-19 lockdown on the optical properties and radiative effects of urban brown carbon aerosol, Geosci. Front., 13, 101320, https://doi.org/10.1016/j.gsf.2021.101320, 2022.

Zhao, R., Lee, A. K. Y., Huang, L., Li, X., Yang, F., and Abbatt, J. P. D.: Photochemical processing of aqueous atmospheric brown carbon, Atmos. Chem. Phys., 15, 6087–6100, https://doi.org/10.5194/acp-15-6087-2015, 2015.

Zhou, S., Collier, S., Xu, J., Mei, F., Wang, J., Lee, Y.-N., Sedlacek, A. J., III, Springston, S. R., Sun, Y., and Zhang, Q.: Influences of upwind emission sources and atmospheric processing on aerosol chemistry and properties at a rural location in the Northeastern US, J. Geophys. Res.-Atmos., 121, 6049–6065, https://doi.org/10.1002/2015jd024568, 2016.